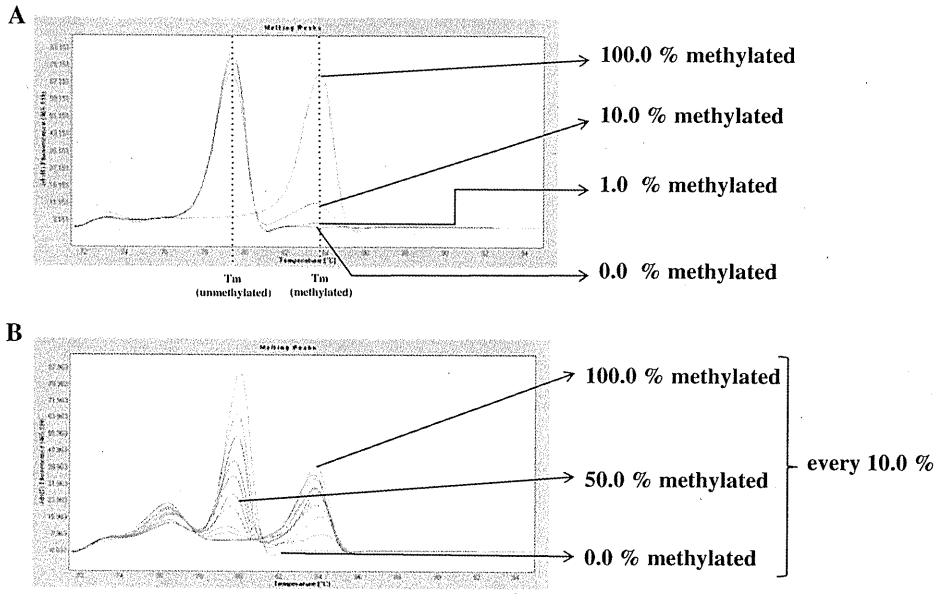

Fig. 1 **A** *MGMT* methylation-sensitive high-resolution melting (MS-HRM) analysis with 100.0% methylated, 0.0% methylated controls, and methylation standards at 10.0 and 1.0% in 0.0% methylated background. Data were analyzed using the Tm calling software module. Two different peaks are obtained for the PCR product derived from the methylated and unmethylated templates. The samples containing a mixture of methylated and unmethylated DNA (methylation standards at 10.0 and 1.0% in 0.0% methylated background) display two peaks. Tm (unmethylated), melting temperature derived from unmethylated DNA; Tm (methylated), melting temperature derived from methylated DNA. **B** *MGMT* MS-HRM analysis with 100.0% methylated, 0.0% methylated, and serially diluted standards at every 10.0%. Data were analyzed using the Tm calling software module

(Table 3). The average methylation level in the 23 methylated samples ranged from 4.1 to 100%. Tumors with a high methylation status (more than 70.0% methylated) were detected in 11 (48%) of the 23 *MGMT*-methylated cases.

Four of five patients with recurrent PCNSLs responded to temozolomide treatment; two cases had a complete response (CR) over 12 months after 1 or 2 cycles of temozolomide, two patients had a partial response (PR), and the remaining patient had progressive disease (Fig. 2). Tumors of all four responders showed relatively high methylation (61.7–99.0%) of the *MGMT* gene (Table 1), and significant *MGMT* methylation was not detected in the patient with progressive disease. In MSP, both unmethylated and methylated *MGMT* were detected in all patients including three cases demonstrated in Fig. 3. It was quite difficult to evaluate the degree of *MGMT* methylation from the result of MSP.

Of the nine cases treated with adjuvant temozolomide after first-line HD-MTX therapy, eight achieved a CR or PR of 7 to 27 months with temozolomide. In addition to HD-MTX and temozolomide, these nine patients received differing treatments (rituximab plus RT in five patients, RT in two patients, rituximab in one patient, and none in one patient). Therefore, we did not investigate the relationship between survival time and methylation status in the patients receiving adjuvant temozolomide.

Table 3 Methylation status of the *MGMT* promoter in 45 PCNSL patients

Degree of *MGMT* promoter methylation (%)[a]	No.
<4.0 (=unmethylated cases)	22
4.1–9.9	3
10.0–19.9	1
20.0–29.9	2
30.0–39.9	2
40.0–49.9	2
50.0–59.9	0
60.0–69.9	2
70.0–79.9	4
80.0–89.9	2
90.0–100.0	5

[a] Percentage of *MGMT* methylation level in our assay

Discussion

The *MGMT* gene is known to be methylated in some systemic B-cell lymphomas [15, 28, 29], but to our knowledge, there has been only one report of *MGMT* methylation in PCNSL[30]. In that study, 6 (60%) of 10 assessable PCNSL patients had methylated MGMT promoters, as measured by gel-based MSP, which is a highly sensitive method to determine epigenetic silencing of genes. As shown in our MSP assay, MSP can detect very low levels

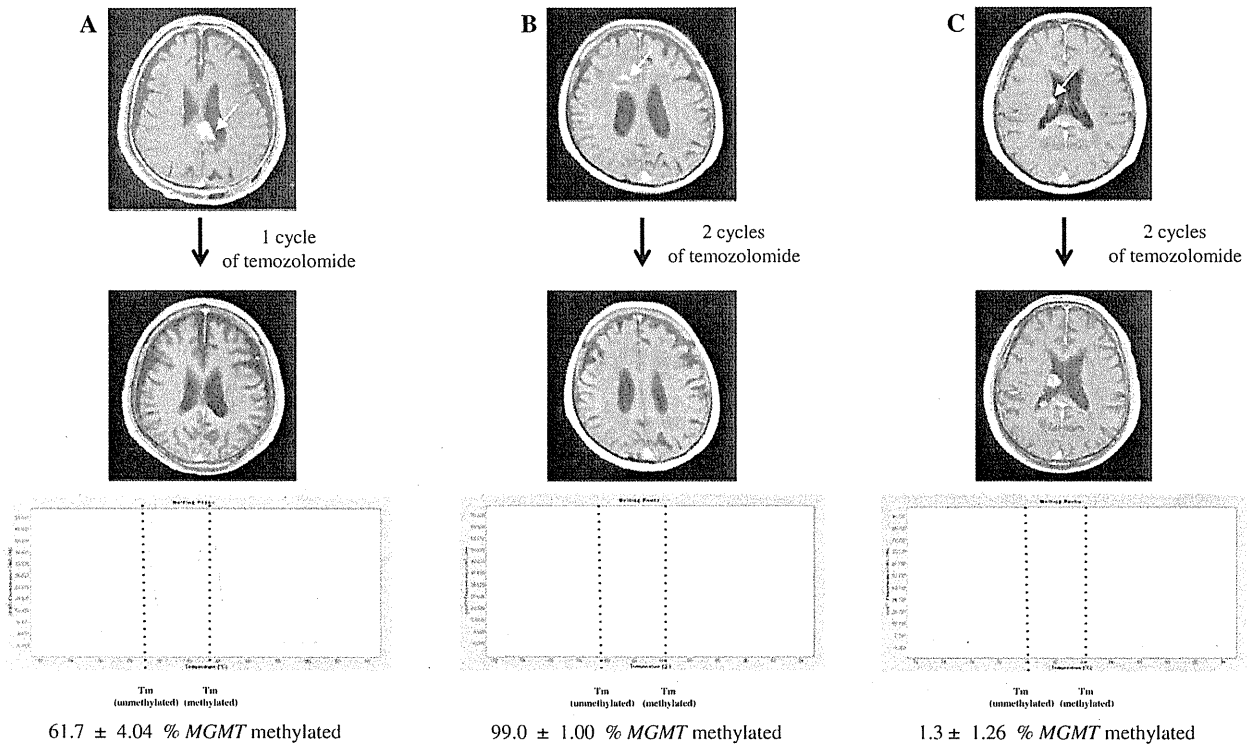

Fig. 2 Relapsed PCNSL cases treated with temozolomide as salvage chemotherapy. **A–C** are cases 1, 2, and 4 in Table 1, respectively. Upper panels show gadolinium-enhanced T1-weighted magnetic resonance images before and after temozolomide treatment. The *white arrows* indicate relapsed tumors. After chemotherapy, tumors completely disappeared in cases 1 and 2, whereas the tumor progressed in case 4. Lower panels show the representative profile of *MGMT* methylation in each case. The mean percentage ± standard deviation of *MGMT* methylation is indicated at the *bottom*

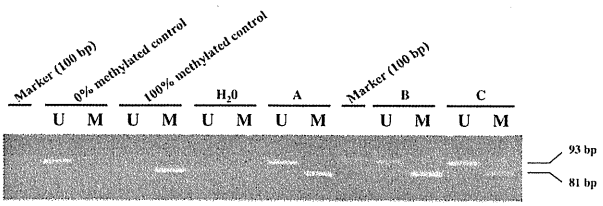

Fig. 3 Methylation-specific PCR results of *MGMT* promoter in cases shown in Fig. 2. PCR products in *lanes* marked as (*U*) indicate the presence of unmethylated *MGMT* alleles. PCR products in *lanes* marked as (*M*) indicate the presence of methylated *MGMT* alleles. 0% methylated control was used as a negative control for methylation, 100% methylated control was used as a positive control for methylation, and water (H_2O) was used as negative PCR control. Marker is a 100 bp DNA marker. The sizes of PCR products are indicated on the right scale. **A–C** are cases 1, 2, and 4 in Table 1, respectively

of DNA methylation or unmethylation. However, several recent studies have raised serious concerns about the application of MSP in a clinical setting. Because of the qualitative nature of the assay, MSP cannot distinguish between high levels of methylation and low levels that have little or no biological significance. Ogino et al. [26] showed that MGMT protein expression was not silenced in tumors with low levels of methylation (less than 4%) in the *MGMT* promoter . Uccella et al. [29] demonstrated that the *MGMT* methylation status correlated with survival in systemic B-cell lymphoma patients treated with alkylating agents; the outcome of survival analysis was unfavorable both in patients with less than 4.0% *MGMT* methylation and in patients with fully unmethylated tumors. Our assay identified some cases with negligible methylation (less than 4.0%), which should have been considered as unmethylated but were defined as methylated by the MSP method. Therefore, it seems reasonable that the *MGMT* methylation frequencies in our series were slightly lower than that found in a previous study using MSP [30]. In addition, a recent study suggested that the MSP assay for *MGMT* methylation is not sufficiently reproducible to make it suitable for clinical use [31]. Thus, a quantitative assay should be used to evaluate *MGMT* promoter methylation in clinical settings. Our study is the first to quantify *MGMT* methylation levels in 45 PCNSLs, which is the largest number of samples reported so far.

Salvage temozolomide treatment has been effective for PCNSL patients who experienced a relapse after HD-MTX chemotherapy. Although cases were small in number, our

results indicate that temozolomide was especially beneficial to patients with tumors containing a highly methylated *MGMT* promoter. Methylation of the *MGMT* promoter is a strong predictor of response, overall survival, and time to disease progression in glioblastoma patients treated with temozolomide [13]. Both the *MGMT* methylation frequency and the proportion of highly methylated tumors are significantly higher for PCNSL than for glioblastoma (our unpublished data), which may explain why PCNSL patients responded to temozolomide. An analysis of more PCNSL patients is needed to evaluate the predictive power of *MGMT* methylation on the impact of salvage temozolomide treatment in PCNSL. Adjuvant therapy with temozolomide is also promising, and a phase III study on the use of HD-MTX and whole brain radiotherapy, with or without concomitant and adjuvant temozolomide, in PCNSL patients is being planned by the Japan Clinical Oncology Group Brain Tumor Study Group.

Acknowledgments This work was supported by a Grant-in-Aid for Scientific Research (C) from the Japan Society for the Promotion of Science (JSPS), 2008–2010. We thank Ms. Kyoko Totake and Mr. Makoto Yamashiro for their technical assistance.

References

1. Herrlinger U, Schabet M, Brugger W, Kortmann RD, Küker W, Deckert M, Engel C, Schmeck-Lindenau HJ, Mergenthaler HG, Krauseneck P, Benöhr C, Meisner C, Wiestler OD, Dichgans J, Kanz L, Bamberg M, Weller M (2002) German Cancer Society Neuro-Oncology Working Group NOA-03 multicenter trial of single-agent high-dose methotrexate for primary central nervous system lymphoma. Ann Neurol 51:247–252
2. Glass J, Gruber ML, Cher L, Hochberg FH (1994) Preirradiation methotrexate chemotherapy of primary central nervous system lymphoma: long-term outcome. J Neurosurg 81:188–195
3. O'Brien P, Roos D, Pratt G, Liew K, Barton M, Poulsen M, Olver I, Trotter G (2000) Phase II multicenter study of brief single-agent methotrexate followed by irradiation in primary CNS lymphoma. J Clin Oncol 18:519–526
4. Treon SP, Chabner BA (1996) Concepts in use of high-dose methotrexate therapy. Clin Chem 42:1322–1329
5. Hoang-Xuan K, Taillandier L, Chinot O, Soubeyran P, Bogdhan U, Hildebrand J, Frenay M, De Beule N, Delattre JY, Baron B, European Organization for Research, Treatment of Cancer Brain Tumor Group (2003) Chemotherapy alone as initial treatment for primary CNS lymphoma in patients older than 60 years: a multicenter phase II study (26952) of the European Organization for Research and Treatment of Cancer Brain Tumor Group. J Clin Oncol 21:2726–2731
6. O'Neill BP, O'Fallon JR, Earle JD, Colgan JP, Brown LD, Krigel RL (1995) Primary central nervous system non-Hodgkin's lymphoma: survival advantages with combined initial therapy? Int J Radiat Oncol Biol Phys 33:663–673
7. Schultz C, Scott C, Sherman W, Donahue B, Fields J, Murray K, Fisher B, Abrams R, Meis-Kindblom J (1996) Preirradiation chemotherapy with cyclophosphamide, doxorubicin, vincristine, and dexamethasone for primary CNS lymphomas: initial report of radiation therapy oncology group protocol 88-06. J Clin Oncol 14:556–564
8. Newlands ES, Stevens MF, Wedge SR, Wheelhouse RT, Brock C (1997) Temozolomide: a review of its discovery, chemical properties, pre-clinical development and clinical trials. Cancer Treat Rev 23:35–61
9. Herrlinger U, Küker W, Platten M, Dichgans J, Weller M (2002) First-line therapy with temozolomide induces regression of primary CNS lymphoma. Neurology 58:1573–1574
10. Lerro KA, Lacy J (2002) Case report: a patient with primary CNS lymphoma treated with temozolomide to complete response. J Neurooncol 59:165–168
11. Omuro AM, Taillandier L, Chinot O, Carnin C, Barrie M, Hoang-Xuan K (2007) Temozolomide and methotrexate for primary central nervous system lymphoma in the elderly. J Neurooncol 85:207–211
12. Reni M, Zaja F, Mason W, Perry J, Mazza E, Spina M, Bordonaro R, Ilariucci F, Faedi M, Corazzelli G, Manno P, Franceschi E, Pace A, Candela M, Abbadessa A, Stelitano C, Latte G, Ferreri AJ (2007) Temozolomide as salvage treatment in primary brain lymphomas. Br J Cancer 96:864–867
13. Hegi ME, Diserens AC, Gorlia T, Hamou MF, de Tribolet N, Weller M, Kros JM, Hainfellner JA, Mason W, Mariani L, Bromberg JE, Hau P, Mirimanoff RO, Cairncross JG, Janzer RC, Stupp R (2005) MGMT gene silencing and benefit from temozolomide in glioblastoma. N Engl J Med 352:997–1003
14. Everhard S, Kaloshi G, Crinière E, Benouaich-Amiel A, Lejeune J, Marie Y, Sanson M, Kujas M, Mokhtari K, Hoang-Xuan K, Delattre JY, Thillet J (2006) MGMT methylation: a marker of response to temozolomide in low-grade gliomas. Ann Neurol 60:740–743
15. Esteller M, Gaidano G, Goodman SN, Zagonel V, Capello D, Botto B, Rossi D, Gloghini A, Vitolo U, Carbone A, Baylin SB, Herman JG (2002) Hypermethylation of the DNA repair gene O(6)-methylguanine DNA methyltransferase and survival of patients with diffuse large B-cell lymphoma. J Natl Cancer Inst 94:26–32
16. Margison GP, Santibanez-Koref MF (2002) O^6-alkylguanine-DNA alkyltransferase: role in carcinogenesis and chemotherapy. Bioessays 24:255–256
17. Gerson SL (2004) MGMT: its role in cancer aetiology and cancer therapeutics. Nat Rev Cancer 4:296–307
18. Karran P, Bignami M (1994) DNA damage tolerance, mismatch repair and genome instability. Bioessays 16:833–839
19. Gerson SL (2002) Clinical relevance of MGMT in the treatment of cancer. J Clin Oncol 20:2388–2399
20. Becker K, Gregel CM, Kaina B (1997) The DNA repair protein O^6-methylguanine-DNA methyltransferase protects against skin tumor formation induced by antineoplastic chloroethylnitrosourea. Cancer Res 57:3335–3338
21. Sakumi K, Shiraishi A, Shimizu S, Tsuzuki T, Ishikawa T, Sekiguchi M (1997) Methylnitrosourea-induced tumorigenesis in MGMT gene knockout mice. Cancer Res 57:2415–2418
22. Danam RP, Qian Howell SR, Brent TP (1999) Methylation of selected CpGs in the human O^6-methylguanine-DNA methyltransferase promoter region as a marker of gene silencing. Mol Carcinog 24(2):85–89
23. Esteller M, Hamilton SR, Burger PC, Baylin SB, Herman JG (1999) Inactivation of the DNA repair gene O^6-methylguanine-DNA methyltransferase by promoter hypermethylation is a common event in primary human neoplasia. Cancer Res 59:793–797
24. Wojdacz TK, Hansen LL (2006) Reversal of PCR bias for improved sensitivity of the DNA methylation melting curve assay. Biotechniques 41:274–278

25. Wojdacz TK, Dobrovic A (2007) Methylation-sensitive high resolution melting (MS-HRM): a new approach for sensitive and high-throughput assessment of methylation. Nucleic Acids Res 35:e41
26. Ogino S, Kawasaki T, Brahmandam M, Cantor M, Kirkner GJ, Spiegelman D, Makrigiorgos GM, Weisenberger DJ, Laird PW, Loda M, Fuchs CS (2006) Precision and performance characteristics of bisulfite conversion and real-time PCR (MethyLight) for quantitative DNA methylation analysis. J Mol Diagn 8:209–217
27. Palmisano WA, Divine KK, Saccomanno G, Gilliland FD, Baylin SB, Herman JG, Belinsky SA (2000) Predicting lung cancer by detecting aberrant promoter methylation in sputum. Cancer Res 60:5954–5958
28. Pike BL, Greiner TC, Wang X, Weisenburger DD, Hsu YH, Renaud G, Wolfsberg TG, Kim M, Weisenberger DJ, Siegmund KD, Ye W, Groshen S, Mehrian-Shai R, Delabie J, Chan WC, Laird PW, Hacia JG (2008) DNA methylation profiles in diffuse large B-cell lymphoma and their relationship to gene expression status. Leukemia 22:1035–1043
29. Uccella S, Cerutti R, Placidi C, Marchet S, Carnevali I, Bernasconi B, Proserpio I, Pinotti G, Tibiletti MG, Furlan D, Capella C (2009) MGMT methylation in diffuse large B-cell lymphoma: validation of quantitative methylation-specific PCR and comparison with MGMT protein expression. J Clin Pathol 62:715–723
30. Kurzwelly D, Glas M, Roth P, Weimann E, Lohner H, Waha A, Schabet M, Reifenberger G, Weller M, Herrlinger U (2009) Primary CNS lymphoma in the elderly: temozolomide therapy and MGMT status. J Neurooncol 97:389–392
31. Vlassenbroeck I, Califice S, Diserens AC, Migliavacca E, Straub J, Di Stefano I, Moreau F, Hamou MF, Renard I, Delorenzi M, Flamion B, DiGuiseppi J, Bierau K, Hegi ME (2008) Validation of real-time methylation-specific PCR to determine O^6-methylguanine-DNA methyltransferase gene promoter methylation in glioma. J Mol Diagn 10:332–337

J Neurooncol (2011) 103:619–627
DOI 10.1007/s11060-010-0433-0

CLINICAL STUDY – PATIENT STUDY

Prediction of malignancy grading using computed tomography perfusion imaging in nonenhancing supratentorial gliomas

Takaaki Beppu · Makoto Sasaki · Kohsuke Kudo · Akira Kurose · Masaru Takeda · Hiroshi Kashimura · Akira Ogawa · Kuniaki Ogasawara

Received: 10 June 2010 / Accepted: 20 September 2010 / Published online: 15 October 2010

Abstract Tumor grade differentiation is often difficult using routine neuroimaging alone. Computed tomography perfusion imaging (CTP) provides quantitative information on tumor vasculature that closely parallels the degree of tumor malignancy. This study examined whether CTP is useful for preoperatively predicting the grade of malignancy in glioma showing no enhancement on contrast-enhanced magnetic resonance imaging (MRI). Subjects comprised 17 patients with supratentorial glioma without enhancement on MRI. CTP was performed preoperatively, and absolute values and normalized ratios of parameters were calculated. Postoperatively, subjects were classified into two groups according to histological diagnosis of grade 3 (G3) glioma or grade 2 (G2) glioma. Absolute values and normalized ratios for each parameter were compared between G3 and G2. Accuracies of normalized ratios for cerebral blood flow (*n*CBF) and cerebral blood volume (*n*CBV) in predicting a diagnosis of G3 were assessed. In addition, *n*CBV was compared between diffuse astrocytoma, G2 oligodendroglial tumor (OT), and G3 OT. Values for *n*CBF and *n*CBV differed significantly between G3 and G2. Using *n*CBV of 1.6 as a cutoff, specificity and sensitivity for distinguishing G3 were 83.3% and 90.9%, respectively. No significant difference in *n*CBV was seen between diffuse astrocytoma and G2 OT, whereas differences were noted between G2 and G3 OTs, and between diffuse astrocytoma and G3 OT. CTP offers a useful method for differentiating between G3 and G2 in nonenhancing gliomas.

Keywords Computed tomography perfusion imaging · Diffuse astrocytoma · Glioma · Nonenhancement · Oligodendroglioma · Preoperative diagnosis

T. Beppu (✉) · M. Takeda · H. Kashimura · A. Ogawa · K. Ogasawara
Department of Neurosurgery, Iwate Medical University, Uchimaru 19-1, Morioka 020-8505, Japan
e-mail: tbeppu@iwate-med.ac.jp

M. Sasaki · K. Kudo
Advanced Medical Research Center, Iwate Medical University, Morioka, Japan

A. Kurose
Department of Pathology, Iwate Medical University, Morioka, Japan

Introduction

Glioma is graded according to World Health Organization (WHO) classification, with grade 1 or 2 graded as low-grade glioma (LGG) and grade 3 or 4 commonly defined as high-grade glioma (HGG) [1]. As treatment and prognosis differ substantially between LGG and HGG, the ability to differentiate between grade 2 (G2) glioma and grade 3 (G3) glioma, as the border between LGG and HGG, is very important. On contrast-enhanced computed tomography (CT) and magnetic resonance imaging (MRI), G2 gliomas are nonenhanced due to preservation of blood–brain barrier (BBB), whereas G3 gliomas are commonly enhanced due to increased vascular permeability caused by disruption of the BBB within the tumor [2–4]. However, the relationship between histological grading and contrast enhancement on CT and MRI is not always clear. Preoperatively differentiating between G3 and G2 gliomas that are nonenhanced on conventional neuroimaging is often difficult. When patients with nonenhancing glioma are encountered, neurooncologists may perform various examinations to differentiate between G3 and G2 gliomas, such as positron emission tomography (PET) for direct assessment of tumor

metabolism, magnetic resonance spectroscopy to detect magnetic resonance signals of metabolites, and diffusion-weighted MRI to clarify structures within and surrounding the tumor. Assessment of intratumoral vasculature is one approach that may help to clarify the intratumoral biological characteristics and malignancy of a tumor, as intratumoral angiogenesis and high vascularity, which are regulated by hypoxia and various vascular endothelial growth factors, are essential for tumor growth and progression [5–7].

Angiography enables direct observation of intratumoral vessels, but is hazardous and remains limited for depiction of intratumoral microvasculature. Magnetic resonance perfusion imaging (MRP) and CT perfusion imaging (CTP) provide reliable information on the intratumoral microvasculature [8–12]. Numerous studies of perfusion imaging have shown that increasing malignancy of the glioma is associated with increased intratumoral blood volume and vascular permeability [10, 13–15]. Quantitative evaluation from perfusion imaging thus depends on both the microvasculature (vascular density and diameter), and vascular permeability due to disruption or absence of the BBB within the tumor. Previous reports have shown good correlations between findings on perfusion imaging and malignancy grading in enhancing glioma. In contrast, the BBB of vessels is preserved in nonenhancing glioma, since extravasation of contrast medium through the BBB in tumor vessels is considered to represent the main cause of tumor contrast enhancement [4]. As MRI remains the preferred technique for assessing brain tumors, studies using MRP to thoroughly evaluate gliomas greatly outnumber those using CTP, and MRP has also been applied to neurooncological applications for nonenhancing gliomas, such as determining biopsy targets and predicting malignant progression [16–18]. In recent years, CTP has gained acceptance as a valuable imaging technique for assessing hemodynamics in brain tumors [13, 14, 19–22]. However, whether CTP is useful for grading malignancy of nonenhancing gliomas remains unclear. CTP retains the advantage of a linear relationship between attenuation changes on CT and tissue concentration of contrast medium, unlike MRP [8, 20]. We therefore hypothesized that CTP should accurately provide quantitative information on only the microvasculature within the tumor, excluding extravasation due to permeability, when limited to patients with nonenhancing glioma. In the present study, we performed CTP on patients with nonenhancing glioma, and compared cerebral blood volume (CBV), cerebral blood flow (CBF), and mean transit time (MTT), as quantitative values provided from CTP, with postoperative histological diagnosis. The present study aims to determine whether CTP is useful for prediction of preoperative malignancy grading (WHO G2 or G3) in nonenhancing glioma on contrast-enhanced MRI.

Patients and methods

Patients

The study protocol was approved by the Ethics Committee of Iwate Medical University, Morioka, Japan. Consecutive patients admitted to the Department of Neurosurgery at Iwate Medical University between September 2006 and January 2010 and meeting the entry criteria were recruited to this study. Entry criteria for this study comprised: diagnosis of supratentorial glioma; tumor bulk not clearly enhanced on gadolinium-enhanced T1-weighted MRI (Gd-T1WI); tumor bulk sited in the supratentorial cerebrum; no past history relating to the brain, including surgical operation, irradiation, administration of anticancer agents or steroids, stroke, infection, or other disorders such as demyelinating disease; and provision of written informed consent to participate. Subjects comprised 17 patients (7 men, 10 women) with mean age of 47.8 years. Patient data including age, tumor site, operation method, postoperative histological diagnosis, and malignancy grade are summarized in Table 1.

Table 1 Patient summary

No.	Age (years)	Tumor site	Surgery	Histology	WHO grade
1	76	Temporal lobe	Biopsy	AA	3
2	58	Frontal lobe	Resection	AO	3
3	45	Frontal lobe	Resection	AO	3
4	34	Frontal lobe	Resection	AO	3
5	29	Frontal lobe	Resection	AO	3
6	21	Frontal lobe	Resection	AOA	3
7	78	Frontal lobe	Biopsy	DA	2
8	68	Frontal lobe	Biopsy	DA	2
9	68	Parietal lobe	Biopsy	DA	2
10	65	Frontal lobe	Resection	DA	2
11	58	Frontal lobe	Resection	DA	2
12	52	Frontal lobe	Resection	Oli	2
13	46	Temporal lobe	Resection	Oli	2
14	42	Frontal lobe	Resection	OA	2
15	30	Frontal lobe	Resection	OA	2
16	27	Frontal lobe	Resection	DA	2
17	16	Temporal lobe	Resection	OA	2

AA anaplastic astrocytoma, *AO* anaplastic oligodendroglioma, *AOA* anaplastic oligoastrocytoma, *DA* diffuse astrocytoma, *Oli* oligodendroglioma, *OA* oligoastrocytoma

Conventional MRI and CTP

Conventional MRI was performed for all subjects within 7 days before surgery. Spin-echo Gd-T1WI was performed approximately 2 min after intravenous injection of gadolinium (0.2 ml/kg, Magnevist; Bayer Schering Pharma, Berlin, Germany), using a 3.0-T whole-body scanner (GE Yokogawa Medical Systems, Tokyo, Japan) with a standard head coil. We confirmed that the tumor in each patient did not show clear enhancement with gadolinium on Gd-T1WI.

CTP was also performed within 7 days before surgery using a 16-row multidetector CT system (Aquillion 16; Toshiba Medical Systems, Tokyo, Japan), in accordance with the methods described by Sasaki et al. [23]. After performing noncontrast CT to determine the location of the tumor balk, a multislice scan targeting the tumor bulk was performed (80 kV_p; 40 mA; 1.5 s/rotation, 30 rotations field of view, 240 × 240 mm^2; four contiguous 8-mm-thick sections; total scan time, 45 s). Five seconds after intravenously injecting 40 ml (4 ml/s) nonionic iodine contrast medium (Iopamiron 300; Bayer Schering Pharma) using a power injector, dynamic scanning was started and tissue attenuation of contrast medium was monitored on a slice. Radiation doses for the scanning protocol were as follows: volume CT dose index, 150 mGy; dose–length product, 480 mGy cm; and effective dose, 1.34 mSv. Data were transferred to a commercial workstation (M900 Quadra; Ziosoft, Tokyo, Japan), and scaled color maps for CBF, CBV, and MTT were automatically created. All mathematical analyses were performed by the deconvolution method [19, 24], using CTP analysis software supplied with the workstation described above. Among the three types of deconvolution algorithms implemented in this software, we used the block-circulant singular value decomposition method. Regions of interest (ROI) for venous output and arterial input functions were manually placed at the superior sagittal sinus and a single branch of the insular segment of the middle cerebral artery on either the pathological or nonpathological side, or A2 segment of the anterior cerebral artery, respectively. ROI were also placed over the entire tumor bulk and apparently normal white matter (ANWM) on the nonpathological side, on color maps for each parameter. Size of the ROI for ANWM was established as 1.0 cm^2. In the measurement of absolute values, the vascular-pixel elimination (VPE) method was used to exclude pixels from large vessels at the cerebral surface, sulci, and cisterns [23, 25]. In the present study, we established the VPE threshold as 6.0 ml/100 g for CBV, since high-CBV areas suggesting large cortical vessels on color map disappeared satisfactorily at 6.0 ml/100 g when the threshold was varied between 5.0 and 8.0 ml/100 g using our analysis software. Large vascular pixels were thus defined as pixels with CBV values >6.0 ml/100 g and were automatically eliminated. Regional absolute values (*r*CBF, *r*CBV, and *r*MTT) were then calculated automatically for all ROI. The measurements described above were performed twice for each patient by two investigators (M.S. and K.K.) who were blinded to all clinical data, including individual patient information and histological diagnosis. Absolute values of all parameters for each patient were determined as the mean of four measured values, as determined twice by each investigator. The second test was performed 1 week after the first test, with a different randomized order of measurements from the first test. We also calculated normalized ratios (*n*CBF, *n*CBV, and *n*MTT) as the absolute value for the tumor divided by the absolute value for the ANWM for each parameter in all patients. All patients underwent surgery, with tumor resection for 13 patients and CT-guided stereotactic needle biopsy for 4 patients (Table 1). The region targeted in stereotactic biopsy was based on findings from the CBV color map. If the color map showed heterogeneous perfusion within the tumor, the targeted region corresponded to the region with the highest perfusion area for CBV. In cases with tumor resection, histological diagnosis was determined by observation at the lesion showing the most malignant histological features in all preparations. Postoperatively, histological diagnosis using specimens obtained from surgery was made by one of the investigators (A.K.) with no prior knowledge of CTP data.

Statistical analyses

All data were analyzed using PASW Statistics version 18 software (SPSS Japan, Tokyo, Japan). Inter- and intrarater reliabilities for all absolute values were evaluated according to classification of the intraclass correlation coefficient (ICC) [26]. For $ICC_{(1,1)}$ and $ICC_{(1,k)}$ as interrater reliability, agreement of all absolute values (CBF, CBV, and MTT) between first and second tests was analyzed for tumor and ANWM for each investigator, using one-factor analysis of variance (ANOVA). For $ICC_{(2,1)}$ and $ICC_{(2,k)}$ as intrarater reliability, agreement of all absolute values between the two investigators was analyzed for tumor and ANWM for each test, using two-factor ANOVA. Patients were assigned to one of two histological grading groups according to histological classification: WHO G2 or WHO G3. Frequency of biopsy was compared between G2 and G3 groups using Fisher's exact probability test. We compared absolute values from the tumor lesion for each parameter between G2 and G3 using the Mann–Whitney *U* test. Furthermore, the normalized ratio for each parameter was compared between these groups again using the Mann–Whitney *U* test. The accuracy of *r*CBF and *n*CBV in predicting a diagnosis of G3 was assessed using receiver

operating characteristic (ROC) curves. ROC curves were calculated in increments of 0.1. Absolute values and normalized ratios for CBV were compared between diffuse astrocytoma, G2 oligodendroglial tumor (OT), and G3 OT, using the Mann–Whitney *U* test. G2 OTs comprised oligodendroglioma or oligoastrocytoma, whereas G3 OTs comprised anaplastic oligodendroglioma or anaplastic oligoastrocytoma. Statistical significance was established at the $P < 0.05$ level in all analyses.

Results

Based on histological diagnosis after surgery, 6 patients were assigned to the G3 group and 11 patients were assigned to the G2 group (Table 1). Of these 17 patients, 4 patients underwent stereotactic biopsy. Frequency of biopsy did not differ significantly between G3 and G2 groups ($P = 0.25$).

Interrater reliability was classified as "almost perfect" for both tumor and ANWM for each investigator: $ICC_{(1,1)}$ and $ICC_{(1,k)}$ for M.S. were 0.943 and 0.971 for tumor, and 0.961 and 0.980 for ANWM, respectively, and those for K.K. were 0.966 and 0.983 for tumor, and 0.942 and 0.970 for ANWM, respectively. Intrarater reliability was also classified as "almost perfect" for both tumor and ANWM in each test: $ICC_{(2,1)}$ and $ICC_{(2,k)}$ in the first test were 0.987 and 0.993 for tumor, and 0.973 and 0.987 for ANWM, respectively, and those in the second test were 0.971 and 0.985 for tumor, and 0.973 and 0.986 for ANWM, respectively. Absolute values of tumor lesions for each parameter in G3 and G2 groups are summarized in Table 2. Absolute values for all parameters varied widely, with no significant differences in any parameters identified between G3 and G2 groups. Normalized ratios for each parameter are summarized in Table 3. Significant differences between G3 and G2 groups were identified for *n*CBF and *n*CBV, with no significant differences in *n*MTT.

The cutoff for accuracy was defined as the point lying closest to the upper-left corner of the ROC curve.

Table 2 Absolute values for each parameter

	*r*CBF (ml/100 g/min)	*r*CBV (ml/100 g)	*r*MTT (s)
G3 ($n = 6$)			
Range	10.8–27.0	1.9–3.2	6.8–10.8
Mean ± SD	18.3 ± 5.3	2.5 ± 0.5	8.5 ± 1.5
G2 ($n = 11$)			
Range	8.8–23.3	1.3–2.6	7.0–12.2
Mean ± SD	15.5 ± 4.2	2.1 ± 0.4	8.8 ± 1.5
P	0.27	0.25	0.76

SD standard deviation

Table 3 Normalized ratios for each parameter

	*n*CBF	*n*CBV	*n*MTT
G3 ($n = 6$)			
Range	1.34–3.00	1.54–2.39	0.76–1.06
Mean ± SD	2.10 ± 0.57	1.92 ± 0.37	0.90 ± 0.12
G2 ($n = 11$)			
Range	0.92–2.00	0.91–1.75	0.79–1.07
Mean ± SD	1.41 ± 0.38	1.26 ± 0.28	0.91 ± 0.09
P	0.01	0.004	0.76

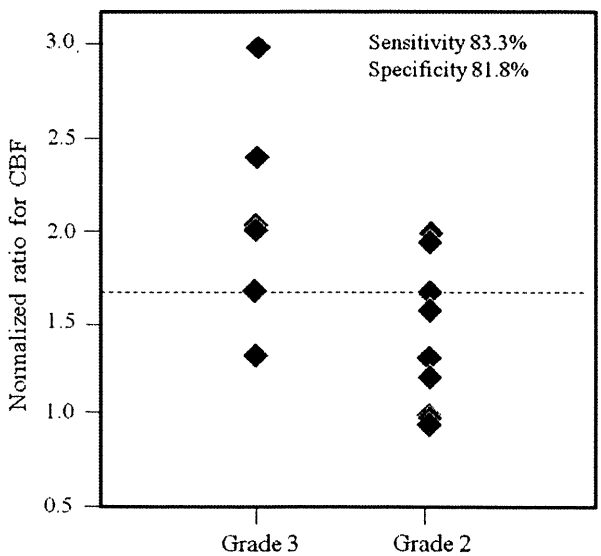

Fig. 1 Relationship between *n*CBF value and WHO grading. Using a cutoff of 1.7 (*dashed line*), *n*CBV was ≥1.7 for 5 (83.3%) of 6 patients with G3, compared with <1.7 for 9 (63.6%) of 11 patients with G2

Sensitivity and specificity in predicting a diagnosis of G3 were 83.3% and 81.8% for *n*CBF (cutoff 1.7), and 83.3% and 90.9% for *n*CBV (cutoff 1.6) (Figs. 1, 2). Accuracy for predicting a diagnosis of G3 was higher with *n*CBV than with *n*CBF.

A comparison of *n*CBV was made between G3 OT, G2 OT, and diffuse astrocytoma (Table 4). Significant differences in *n*CBV were identified between G3 and G2 OTs ($P = 0.009$), and between G3 OT and diffuse astrocytoma ($P = 0.02$), whereas no significant difference was seen between G2 OT and diffuse astrocytoma ($P = 0.36$).

Illustrative cases

We now describe the cases of two patients for whom CTP provided useful information for predicting tumor grading. Gd-T1WI for case 6 showed glioma with no clear enhancement in the right frontal lobe (Fig. 3a). Using the

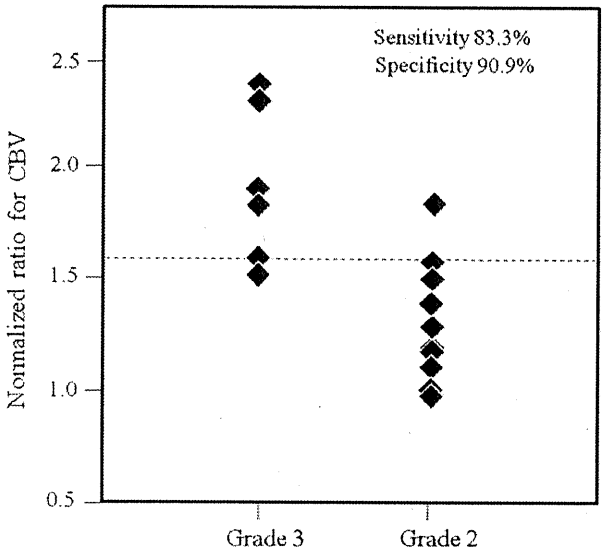

Fig. 2 Relationship between *n*CBV value and WHO grading. Using a cutoff point of 1.6 (*dashed line*), *n*CBV was ≥1.6 for 5 (83.3%) of 6 patients with G3 and <1.6 for 10 (90.9%) of 11 patients with G2

Table 4 Normalized ratio (mean ± SD) for CBV in G3 OT, G2 OT, and diffuse astrocytoma

	*n*CBV
G3 OT ($n = 5$)	1.99 ± 0.36
G2 OT ($n = 5$)	1.16 ± 0.24
Diffuse astrocytoma ($n = 6$)	1.35 ± 0.31

OT oligodendroglial tumors

VPE method, color mapping of CBV demonstrated large vessels of the cerebral surface to be successfully excluded (Fig. 3b). Color mapping of CBV depicted areas of hyperperfusion within the tumor. The *n*CBV for this case (*n*CBV = 2.3) was higher than the cutoff point. Tissue specimens obtained from gross total resection showed typical histological features of G3 anaplastic oligoastrocytoma.

Gd-T1WI for case 14 showed nonenhancing glioma of the right frontal lobe (Fig. 4a). The VPE method satisfactorily eliminated large vessels of the cerebral surface (Fig. 4b). On color mapping, areas of hyperperfusion seemed to be minor compared with those in case 6. The *n*CBV in this case (*n*CBV = 1.2) was lower than the cutoff point. After tumor resection, histological diagnosis was G2 oligoastrocytoma.

Discussion

Previous reports have documented that G3 gliomas make up 40–46% of nonenhancing gliomas on conventional MRI [3, 4]. Our finding of G3 tumors in 6 (35.2%) of 17 patients

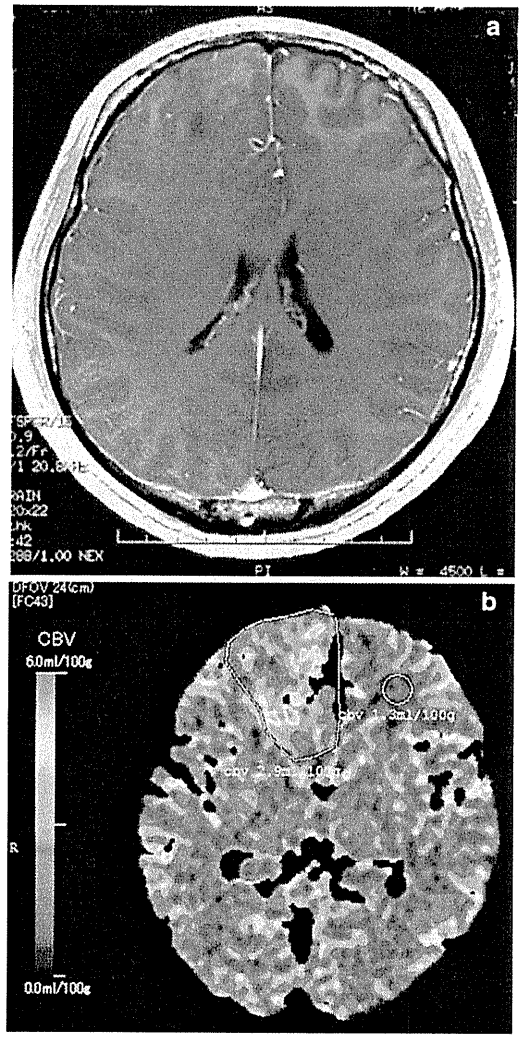

Fig. 3 Gd-T1WI (**a**) and color map of CBV (**b**) for case 6. *Circle* ROI covering the entire tumor bulk and ANWM localized on the nonpathological side

was close to this level. Thus, preoperative differentiation between G3 and G2 using MRI is often difficult. Biopsy or resection allowing histological diagnosis currently remain the basis for differentiation between G3 and G2 gliomas. However, neuroimaging can provide useful information on pathological diagnosis, particularly for patients who do not undergo biopsy or resection allowing histological diagnosis. Novel neuroimaging procedures other than routine MRI are thus desired. CTP and MRP provide reliable information on tumor vasculature, which can help to determine the extent of malignancy in glioma [8, 10, 22]. Although limitations of CTP include radiation dose and limited area of coverage compared with MRP, the linear relationship between attenuation changes on CT and tissue concentration of contrast medium and the lack of confounding sensitivity to flow artifacts allow CTP to

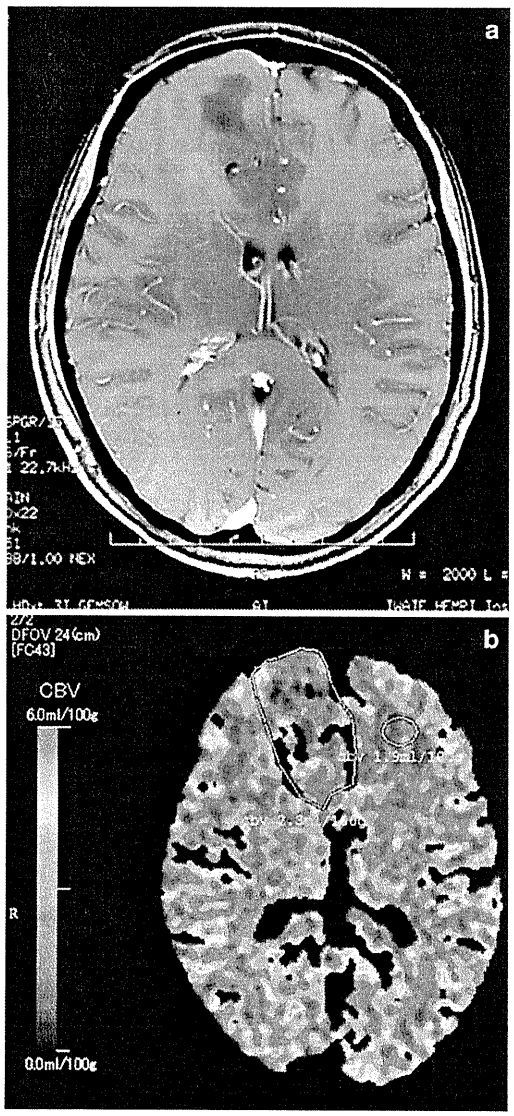

Fig. 4 Gd-T1WI (**a**) and color map of CBV (**b**) for case 14. *Circle* ROI covering the entire tumor bulk and ANWM localized on the nonpathological side

potentially offer a more accurate representation of tissue microvasculature than similar MRP studies [8, 20]. Furthermore, CTP offers advantages such as measurement of quantitative absolute values, greater availability, fast scanning time, high spatial resolution, low cost, and the ability to use this technique for patients who cannot undergo MRI due to the presence of metallic materials in the body [14, 22, 27].

CBF derived from CTP has been suggested to show a tendency toward overestimation, compared with that derived from PET [28]. Since overestimation of CBF in CTP was attributable to the presence of large vessels on the cerebral surface, as contrast materials act as a nondiffusible intravascular tracer in CTP unlike in PET, the VPE method has been proposed to eliminate flow in large vessels [25]. Accurate measurement of CBV contributes to accurate CBF and MTT, as these parameters are closely associated in the central volume principle as CBF = CBV/MTT [29]. We therefore used the VPE method in the present study. We think that optimal threshold differs according to the specific analysis software used for CTP. While VPE threshold was 8.0 ml/100 g in the report by Kudo et al. [25], we established a threshold of 6.0 ml/100 g, since high-CBV areas from cortical large vessels disappeared satisfactorily at this threshold for the analysis software used in our study. Another reason for using the VPE method is that OTs are commonly seen as superficially located tumors in the brain [30, 31]. Elimination of superficial large vessels at the cerebral surface, sulci, and cisterns thus seems warranted when CTP is performed for OTs.

In previous reports of CTP, *r*CBV values ranged from 2.3 to 8.87 ml/100 g for HGG and from 0.95 to 3.28 ml/100 g for LGG, differing significantly between HGG and LGG [13, 14, 20]. The present mean rCBV values in G3 and G2 (Table 2) agreed with previous findings. In addition, mean rCBV values in both G3 and G2 were less than half of 6.0 ml/100 g as VPE threshold. These findings suggest that the VPE method used in this study did not exclude tumor vessels along with other large vessels from CBV maps. While *r*CBV for G3 tended to be on the low side compared with previous reports, this could have resulted from the exclusion of patients with enhancing glioma as subjects in this study. Extravasation of contrast medium through the BBB in enhanced glioma may directly lead to increased CBV, due to the linear relationship between attenuation changes on CT and tissue concentration of contrast medium. Jain et al. [20] documented that *r*CBF and *r*CBV in nonenhancing G3 glioma do not differ significantly from those in nonenhancing G2 glioma, although sample size in that report was small. The present study with more subjects suggested that even nonenhancing G3 glioma retains more vascular density than G2, although the difference in *r*CBV between the two groups was minor (Table 2). However, this result might have been influenced by the disproportionate number of OTs in the G2 (42%) and G3 (83%) groups. If vascular density is significantly higher in G3 OT than in anaplastic astrocytoma, the large number of G3 OTs may have result in a high mean CBV for the G3 group in this study. This issue represents a definite limitation to the present study.

Concentration of contrast medium within the tumor might be subtly influenced by individual parameters such as body size and cardiac output volume, and differences in analytical software among institutes. We must emphasize the importance of estimation using normalized ratios, as

this allows us to ignore these differences. Ellika et al. [22] reported findings for *n*CBV using CTP in 19 patients with glioma, composed of a mixture of enhancing and nonenhancing WHO G1–G4 gliomas, and the utility of *n*CBF and *n*CBV for distinguishing HGG from LGG. They also documented *n*CBF and *n*CBV ranges of 0.78–3.75 and 1.5–3.7 in two patients with nonenhancing G3 glioma, and ranges of 1.26–1.48 and 0.94–1.72 in three patients with nonenhancing G2 glioma, respectively. Mean values of *n*CBF and *n*CBV in G3 and G2 in this study (Table 3) seemed close to the values reported by Ellika et al.

Radiographic grading of gliomas with conventional MRI is not always accurate, with 85.7% sensitivity for predicting HGG, even when including subjects with enhancing glioma [22]. When subjects are limited to those with nonenhancing gliomas, radiographic grading using conventional MRI should be more difficult. A previous report documented 85.7% sensitivity and 100% specificity for identifying HGG using *n*CBV [22]. In the present study, CTP could distinguish nonenhancing G3 glioma from nonenhancing G2 glioma with 83.3% sensitivity and 90.9% specificity using *n*CBV (Fig. 2). This was superior to the results for *n*CBF. Accuracy for distinguishing G3 using *n*CBV in the present study was by no means inferior to that reported by Ellika et al. [22], but subjects in this study were limited to those with nonenhancing glioma. These results suggest that *n*CBV in CTP is useful as an auxiliary examination in addition to routine neuroimaging for predicting the grade of malignancy in nonenhancing gliomas.

Previous studies using MRP have documented higher relative CBV in OT than in other gliomas [32–34]. Lev et al. [33] suggested that OTs tend to appear as high blood volume lesion on MRP, without respect to tumor grade. Two reports using MRP documented that G2 OTs show higher relative CBV than diffuse astrocytoma [32, 34]. Also in a report using CTP by Narang et al. [15], G2 OTs showed a trend towards higher CBV than G2 astrocytic tumors, although no significant difference was found, and no significant difference in CBV between G3 OTs and G2 OTs was identified. Those reports explained the high relative CBV of OT by a hypothesis based on the specific histological features of fine capillary networks [33]. Furthermore, those reports suggested that grading malignancy may be difficult when patients with OT are included, due to a high relative CBV. In the present study, no significant difference in *n*CBV was seen between diffuse astrocytoma and G2 OT, whereas significant differences were found between G3 OT and G2 OT. The difference between the reports described above and the present investigation might be explained by differences between MRP and CTP, and by the use of the VPE method in this study. Signal changes in dynamic susceptibility contrast (DSC) MRI for MRP do not depend on only the concentration of contrast material, but also on T2* or T2 relaxation rates, which are affected by calcified foci and hemorrhage within tumor tissue. These histological features are commonly seen in OTs. DSC signals might thus be higher in OTs than in diffuse astrocytoma, even when the microvascular densities are comparable. The VPE method may have eliminated pixels of high-CBV vessels in OTs, if vascular density in OTs is significantly higher than that in diffuse astrocytoma. However, exclusion of large vessels at the cerebral surface and sulci from CTP maps is important, as OTs grow superficially in the brain. Cha et al. [32] explained for reason of high relative CBV for OTs in MRP by the predominant cortical location in addition to distinct vascular pattern in OTs. We think that CTP with the VPE method is useful for simple malignancy grading in subjects with OTs. Conversely, MRP offers potential advantages for the diagnosis of OTs. However, CTP should not be performed additionally to MRP if the purpose in examination is achieved by MRP, as CTP retains drawbacks such as radiation dose and iodine contrast medium.

The present study possesses some limitations regarding the interpretation of study results. First, the number of patients in this study was small, with remarkably fewer cases of anaplastic astrocytoma compared with OT in G3, as mentioned above. Further investigation including a larger number of cases of anaplastic astrocytoma is needed. A second limitation is the possible discrepancy between histological diagnosis and the region of highest CBV within the tumor. The region targeted for stereotactic biopsy was not rigorously transferred from the region of highest *r*CBV ("hot spots"). However, risk of histological misdiagnosis caused by sampling error during biopsy might be negligible, since the number of patients who underwent biopsy was small in both G3 and G2, and no significant difference in frequency of biopsy was seen between groups. In patients who underwent tumor resection, histological diagnosis was not made using tissue specimens rigorously corresponding to "hot spots." However, histological diagnosis based on the most malignant histological features should be closely associated with high CBV, as increased malignancy is associated with higher vascular density. CTP with a 16-row multidetector CT scanner, covering only four contiguous 8-mm-thick sections, did not cover the entire tumor bulk in some patients. For those patients, histological diagnosis was made using tumor tissues corresponding to the area depicted in CTP. A third limitation was that data calculated from CTP in this study were not the highest CBV values for a small ROI placed in "hot spots" on a color map, but rather were mean values for a large ROI covering the entire tumor bulk. This issue also influences the second limitation. We thought that the simple protocol in this study, combining absolute values as a mean in a large ROI with histological diagnosis from the

area of the most malignant features, is suitable for application in clinical practice, as tissue sampling error of regions corresponding to a small ROI can be avoided. High ICC in inter- and intrarater reliabilities showed that the protocol used in this study offers high reproducibility.

Conclusions

We performed CTP combined with the VPE method for 17 patients, to clarify whether CTP can accurately differentiate between G3 and G2 nonenhancing glioma. Our results showed that *n*CBV from CTP was highly accurate in differentiating G3 from G2 nonenhancing gliomas. The most important result was that CTP enabled differentiation between G3 and G2 nonenhancing OTs. CTP combined with the VPE method offers a useful technique for differentiating between G3 and G2 in nonenhancing gliomas.

Acknowledgments This study was supported in part by a Grant-in-Aid for Advanced Medical Science Research from the Ministry of Science, Education, Sports, and Culture, Japan.

References

1. Louis DN, Ohgaki H, Wiestler OD, Cavenee WK, Burger PC, Jouvet A, Scheithauer BW, Kleihues P (2007) The 2007 WHO classification of tumours of the central nervous system. Acta Neuropathol 114:97–109
2. Dean BL, Drayer BP, Bird CR, Flom RA, Hodak JA, Coons SW, Carey RG (1990) Gliomas: classification with MR imaging. Radiology 174:411–415
3. Ginsberg LE, Fuller GN, Hashmi M, Leeds NE, Schomer DF (1998) The significance of lack of MR contrast enhancement of supratentorial brain tumors in adults: histopathological evaluation of a series. Surg Neurol 49:436–440
4. Mihara F, Numaguchi Y, Rothman M, Kristt D, Fiandaca M, Swallow L (1995) Non-enhancing supratentorial malignant astrocytomas: MR features and possible mechanisms. Radiat Med 13:11–17
5. Jain RK, Gerlowski LE (1986) Extravascular transport in normal and tumor tissues. Crit Rev Oncol Hematol 5:115–170
6. Shweiki D, Itin A, Soffer D, Keshet E (1992) Vascular endothelial growth factor induced by hypoxia may mediate hypoxia-initiated angiogenesis. Nature 359:843–845
7. Vajkoczy P, Menger MD (2000) Vascular microenvironment in gliomas. J Neurooncol 50:99–108
8. Barnett G (2006) High-grade gliomas. Humana, Totowa
9. Law M, Cha S, Knopp EA, Johnson G, Arnett J, Litt AW (2002) High-grade gliomas and solitary metastases: differentiation by using perfusion and proton spectroscopic MR imaging. Radiology 222:715–721
10. Law M, Yang S, Wang H, Babb JS, Johnson G, Cha S, Knopp EA, Zagzag D (2003) Glioma grading: sensitivity, specificity, and predictive values of perfusion MR imaging and proton MR spectroscopic imaging compared with conventional MR imaging. Am J Neuroradiol 24:1989–1998
11. Eastwood JD, Lev MH, Provenzale JM (2003) Perfusion CT with iodinated contrast material. Am J Roentgenol 180:3–12
12. Hoeffner EG, Case I, Jain R, Gujar SK, Shah GV, Deveikis JP, Carlos RC, Thompson BG, Harrigan MR, Mukherji SK (2004) Cerebral perfusion CT: technique and clinical applications. Radiology 231:632–644
13. Ding B, Ling HW, Chen KM, Jiang H, Zhu YB (2006) Comparison of cerebral blood volume and permeability in preoperative grading of intracranial glioma using CT perfusion imaging. Neuroradiology 48:773–781
14. Eastwood JD, Provenzale JM (2003) Cerebral blood flow, blood volume, and vascular permeability of cerebral glioma assessed with dynamic CT perfusion imaging. Neuroradiology 45:373–376
15. Narang J, Jain R, Scarpace L, Saksena S, Schultz LR, Rock JP, Rosenblum M, Patel SC, Mikkelsen T (2010) Tumor vascular leakiness and blood volume estimates in oligodendrogliomas using perfusion CT: an analysis of perfusion parameters helping further characterize genetic subtypes as well as differentiate from astroglial tumors. J Neurooncol. doi:10.1007/s11060-010-0317-3
16. Maia AC Jr, Malheiros SM, da Rocha AJ, Stavale JN, Guimaraes IF, Borges LR, Santos AJ, da Silva CJ, de Melo JG, Lanzoni OP, Gabbai AA, Ferraz FA (2004) Stereotactic biopsy guidance in adults with supratentorial nonenhancing gliomas: role of perfusion-weighted magnetic resonance imaging. J Neurosurg 101:970–976
17. Danchaivijitr N, Waldman AD, Tozer DJ, Benton CE, Brasil Caseiras G, Tofts PS, Rees JH, Jager HR (2008) Low-grade gliomas: do changes in rCBV measurements at longitudinal perfusion-weighted MR imaging predict malignant transformation? Radiology 247:170–178
18. Price SJ (2010) Advances in imaging low-grade gliomas. Adv Tech Stand Neurosurg 35:1–34
19. Nabavi DG, Cenic A, Craen RA, Gelb AW, Bennett JD, Kozak R, Lee TY (1999) CT assessment of cerebral perfusion: experimental validation and initial clinical experience. Radiology 213: 141–149
20. Jain R, Ellika SK, Scarpace L, Schultz LR, Rock JP, Gutierrez J, Patel SC, Ewing J, Mikkelsen T (2008) Quantitative estimation of permeability surface-area product in astroglial brain tumors using perfusion CT and correlation with histopathologic grade. Am J Neuroradiol 29:694–700
21. Jain R, Scarpace L, Ellika S, Schultz LR, Rock JP, Rosenblum ML, Patel SC, Lee TY, Mikkelsen T (2007) First-pass perfusion computed tomography: initial experience in differentiating recurrent brain tumors from radiation effects and radiation necrosis. Neurosurgery 61:778–786
22. Ellika SK, Jain R, Patel SC, Scarpace L, Schultz LR, Rock JP, Mikkelsen T (2007) Role of perfusion CT in glioma grading and comparison with conventional MR imaging features. Am J Neuroradiol 28:1981–1987
23. Sasaki M, Kudo K, Ogasawara K, Fujiwara S (2009) Tracer delay-insensitive algorithm can improve reliability of CT perfusion imaging for cerebrovascular steno-occlusive disease: comparison with quantitative single-photon emission CT. Am J Neuroradiol 30:188–193
24. Wintermark M, Maeder P, Thiran JP, Schnyder P, Meuli R (2001) Quantitative assessment of regional cerebral blood flows by perfusion CT studies at low injection rates: a critical review of the underlying theoretical models. Eur Radiol 11:1220–1230
25. Kudo K, Terae S, Katoh C, Oka M, Shiga T, Tamaki N, Miyasaka K (2003) Quantitative cerebral blood flow measurement with dynamic perfusion CT using the vascular-pixel elimination method: comparison with H2(15)O positron emission tomography. Am J Neuroradiol 24:419–426
26. Shrout PE, Fleiss JL (1979) Intraclass correlations: uses in assessing rater reliability. Psychol Bull 86:420–428
27. Miles KA, Charnsangavej C, Lee FT, Fishman EK, Horton K, Lee TY (2000) Application of CT in the investigation of angiogenesis in oncology. Acad Radiol 7:840–850

28. Gillard JH, Minhas PS, Hayball MP, Bearcroft PW, Antoun NM, Freer CE, Mathews JC, Miles KA, Pickard JD (2000) Assessment of quantitative computed tomographic cerebral perfusion imaging with H2(15)O positron emission tomography. Neurol Res 22: 457–464
29. Meier P, Zierler KL (1954) On the theory of the indicator-dilution method for measurement of blood flow and volume. J Appl Physiol 6:731–744
30. Piepmeier J, Baehring JM (2004) Surgical resection for patients with benign primary brain tumors and low grade gliomas. J Neurooncol 69:55–65
31. Beppu T, Inoue T, Nishimoto H, Ogasawara K, Ogawa A, Sasaki M (2007) Preoperative imaging of superficially located glioma resection using short inversion-time inversion recovery images in high-field magnetic resonance imaging. Clin Neurol Neurosurg 109:327–334
32. Cha S, Tihan T, Crawford F, Fischbein NJ, Chang S, Bollen A, Nelson SJ, Prados M, Berger MS, Dillon WP (2005) Differentiation of low-grade oligodendrogliomas from low-grade astrocytomas by using quantitative blood-volume measurements derived from dynamic susceptibility contrast-enhanced MR imaging. Am J Neuroradiol 26:266–273
33. Lev MH, Ozsunar Y, Henson JW, Rasheed AA, Barest GD, Harsh GR IV, Fitzek MM, Chiocca EA, Rabinov JD, Csavoy AN, Rosen BR, Hochberg FH, Schaefer PW, Gonzalez RG (2004) Glial tumor grading and outcome prediction using dynamic spin-echo MR susceptibility mapping compared with conventional contrast-enhanced MR: confounding effect of elevated rCBV of oligodendrogliomas. Am J Neuroradiol 25:214–221
34. Maia AC Jr, Malheiros SM, da Rocha AJ, da Silva CJ, Gabbai AA, Ferraz FA, Stavale JN (2005) MR cerebral blood volume maps correlated with vascular endothelial growth factor expression and tumor grade in nonenhancing gliomas. Am J Neuroradiol 26:777–783

Neurol Med Chir (Tokyo) 51, 472～476, 2011

Wireless Modification of the Intraoperative Examination Monitor for Awake Surgery

—Technical Note—

Kitaro YOSHIMITSU,[1] Takashi MARUYAMA,[1,2] Yoshihiro MURAGAKI,[1,2] Takashi SUZUKI,[1] Taiichi SAITO,[2] Masayuki NITTA,[2] Masahiko TANAKA,[2] Mikhail CHERNOV,[1,2] Manabu TAMURA,[1] Soko IKUTA,[1] Jun OKAMOTO,[1,2] Yoshikazu OKADA,[2] and Hiroshi ISEKI[1,2]

[1]*Faculty of Advanced Techno-Surgery, Institute of Advanced Biomedical Engineering and Science; and* [2]*Department of Neurosurgery, Neurological Institute; Tokyo Women's Medical University, Tokyo*

Abstract

The dedicated intraoperative examination monitor for awake surgery (IEMAS) was originally developed by us to facilitate the process of brain mapping during awake craniotomy and successfully used in 186 neurosurgical procedures. This information-sharing device provides the opportunity for all members of the surgical team to visualize a wide spectrum of the integrated intraoperative information related to the condition of the patient, nuances of the surgical procedure, and details of the cortical mapping, practically without interruption of the surgical manipulations. The wide set of both anatomical and functional parameters, such as view of the patient's mimic and face movements while answering the specific questions, type of the examination test, position of the surgical instruments, parameters of the bispectral index monitor, and general view of the surgical field through the operating microscope, is presented compactly in one screen with several displays. However, the initially designed IEMAS system was occasionally affected by interruption or detachment of the connecting cables, which sometimes interfered with its effective clinical use. Therefore, a new modification of the device was developed. The specific feature is installation of wireless information transmitting technology using audio-visual transmitters and receivers for transfer of images and verbal information. The modified IEMAS system is very convenient to use in the narrow space of the operating room.

Key words: awake craniotomy, intraoperative cortical mapping, intraoperative monitoring, cerebral glioma, surgery

Introduction

Current management strategy of cerebral gliomas emphasizes the importance of maximal possible surgical resection with minimal risk of postoperative morbidity,[7,11,12] but this goal cannot be attained without use of the advanced computer-assisted intraoperative technologies, because of the typical infiltrative growth and unclear borders of primary parenchymal brain tumors, as well as the common effects on functionally-important cerebral structures, which create a significant challenge for differentiation between the margin of the lesion and adjacent viable normal tissue. Various technological adjuncts directed at facilitation of surgery for intracranial neoplasms are currently incorporated into neurosurgical practice.[4,5] Particularly, the technique of awake craniotomy is widely used for intraoperative brain mapping during resection of lesions located in or in the nearest vicinity to eloquent cortical areas.[8,9,16,20]

Around a decade ago, the dedicated intraoperative examination monitor for awake surgery (IEMAS) was developed by our group.[5,6,11,19] The clinical experience with this device was generally very successful, but a few minor problems still appeared. First, carrying of the IEMAS in and out of the operating room between surgeries easily damaged the connecting cables and attachments, which sometimes resulted in highly undesirable mechanical problems during tumor resection. Sec-

Received December 14, 2010; Accepted March 9, 2011

ond, the quantity of medical information displayed on the screen of IEMAS was not considered adequate by the operating surgeon in some cases. Therefore, the device was improved by modifications. The details of its initial clinical testing was reported previously and published elsewhere.[21] Here we present our clinical experience with routine use.

Materials and Methods

IEMAS was designed as an information-sharing device for use during awake craniotomy for intracranial lesions.[6] The device provides simultaneous real-time visualization of a wide spectrum of intraoperative data. For example, the patient's mimic and face movements during answering specific test questions, type of the examination test, position of the surgical instruments and cortical stimulator in the surgical field, parameters of the bispectral index monitor, and general view of the surgical field through the operating microscope, can be presented compactly in one screen with several displays (Fig. 1). Moreover, this combined image can be projected on several in-room liquid crystal display (LCD) monitors, so the integrated real-time information can be easily distributed and quickly analyzed by all members of the surgical team, practically without interruption of the surgical manipulations.

The specific feature of the new modification of the IEMAS system is the installation of wireless information transmitting technology using audio-visual transmitters and receivers for transfer of images and verbal information.[21] The general technical characteristics are presented in Table 1. The device consists of 3 main parts: patient monitor, operator monitor, and control box (Fig. 2).

The patient monitor is a 3.5-inch LCD with a small

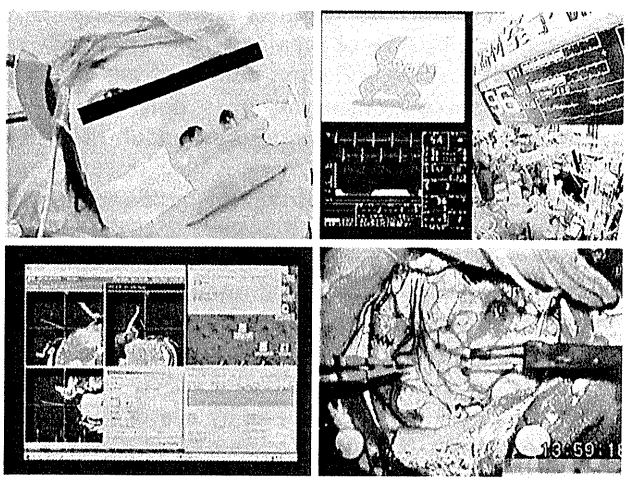

Fig. 1 Integration of multiple intraoperative parameters on the screen of the wireless intraoperative examination monitor for awake surgery. On the *upper left* display, the patient face and eyes can be seen to facilitate checking of the consciousness status and mimics during response to test questions. On the *lower left* display, the anatomical data from the real-time updated neuronavigation system is shown, which can localize the exact position of the cortical stimulator. On the *lower right* display, the view of the surgical field through the operative microscope during brain mapping is seen, which can be helpful for precise identification of the timing of stimulation. On the *upper right* display, 4 different types of information are presented, which are (*clockwise*): the test object provided for a patient for naming, parameters of the bispectral index monitor reflecting the patient's awake state, general view of the operating theater, and parameters of the heart beat monitor. In total, 7 different intraoperative parameters are integrated in real-time on one screen.

Table 1 Technical parameters of the latest modification of intraoperative examination monitor for awake surgery

Size (mm)	390 × 1100 × 1300
Power supply (V)	AC 100; DC 12
Frequency range of audio-visual transmitters	1.2 GHz (1 channel) and 2.45 GHz (2 channels)
Camera and monitors	CCD camera 3.5 inch LCD monitor (patient monitor) 7.5 inch LCD monitor (operator monitor)
Degrees of freedom in monitors positioning	6 (self-controlling)

AC: alternating current, CCD: charge coupled device, DC: direct current, LCD: liquid crystal display.

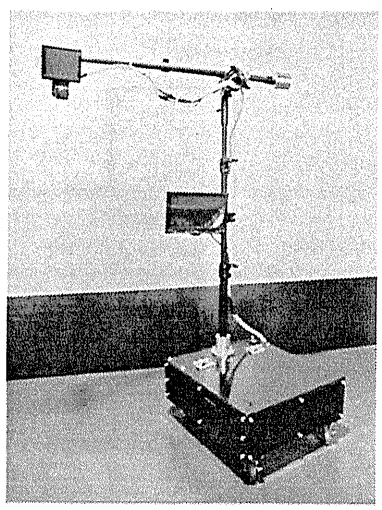

Fig. 2 General view of the wireless modification of intraoperative examination monitor for awake surgery. Three main parts of the device are seen, patient monitor, operator monitor, and control box.

charge coupled device (CCD) camera and incorporated highly sensitive microphone. The test questions for the patient are displayed on this monitor, and the camera images the patient's face simultaneously with the verbal response to tests. The operator monitor is a 7.5-inch LCD, which can project various intraoperative parameters. The whole combined image is constructed with a special divider of the recording system. In the modified IEMAS, 7 separate windows can be created on this screen, compared with 5 on the previous version of the device. The image of this monitor is recorded on the hard disk of the recording system, which is located outside the operating room (Fig. 3). The control box contains a down scan converter, alternating current power supply, and audio-visual transmitters and receivers. Metal poles connecting all 3 components of the device are made from the recreated parts of the commercially available tripod.

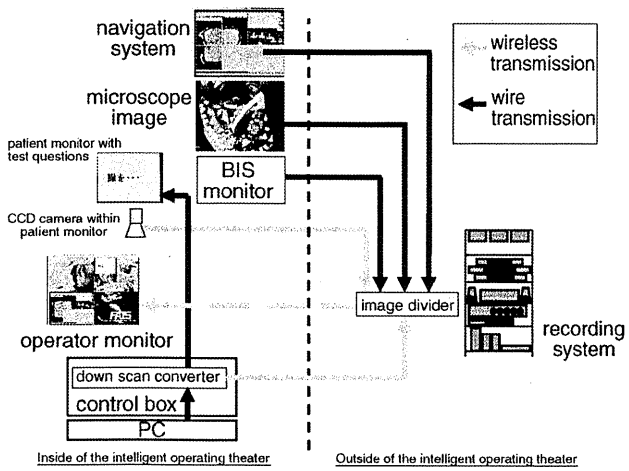

Fig. 3 Scheme of information transfer during use of intraoperative examination monitor for awake surgery and signal exchanging system provided by audio-visual transmitters and receivers. BIS: bispectral index, CCD: charge coupled device, PC: personal computer.

In the operating theater, the compact device is located beside the operating table and controlled by the assistant in charge of brain function monitoring (Fig. 4), whose main tasks include providing of the test questions for the patient simultaneously with electrical stimulation of the cerebral cortex performed by the operating surgeon, and checking the appropriateness of response by evaluation of both the verbal answer and movements of the facial muscles and eyeballs.

Results

A total of 939 neurosurgical procedures for resection of intracranial gliomas were performed in the intelligent operating theater of the Tokyo Women's Medical University from March 2000 to January 2011. Awake craniotomy was performed in 220 cases, and the initial modification of IEMAS was used 186 times.

The clinical testing of the new modification of the device was initiated on February 1, 2010, and immediately revealed the presence of crossed line effects, which resulted in impaired quality of visual and auditory data. This technical trouble was caused by imperfect design of the control box, with close vicinity of the several transmitters and receivers within the same tight space, as well as by use of a similar frequency (2.4 GHz) for all transmitters. Change of the

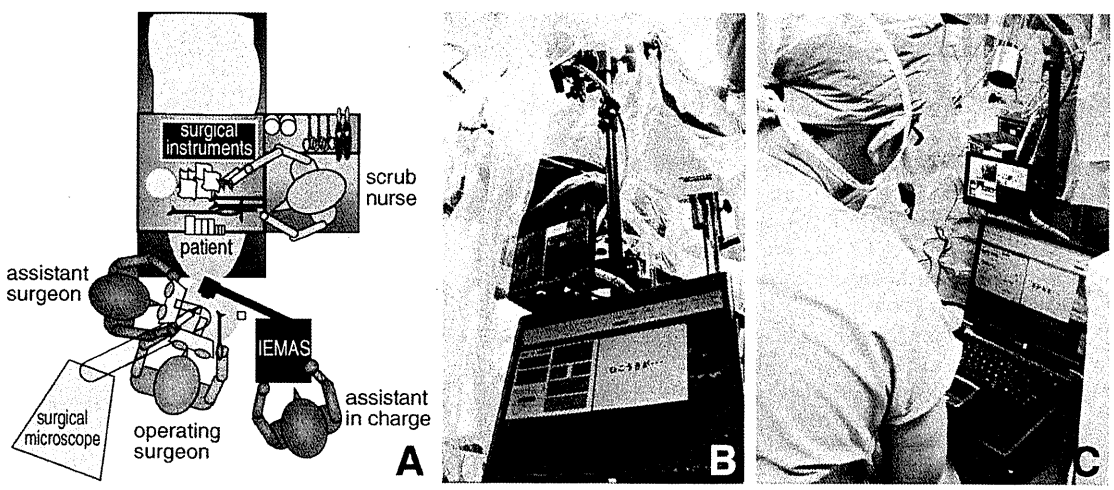

Fig. 4 Schematic (A) and real (B) demonstration of the position of the intraoperative examination monitor for awake surgery (IEMAS) during resection of glioma, and its use by the assistant in charge of brain mapping (C).

Table 2 Possible problems with identification of the speech areas with intraoperative electrical stimulation of the cerebral cortex during awake craniotomy and technical solutions required for their elimination*

Problem	Solution
Speech arrest during intraoperative cortical mapping may be similarly caused by stimulation of the different cortical areas, namely motor cortex, negative motor cortex, and speech area itself, which requires their precise discrimination. Presence of the surgical drapes separating the patient face and examination monitor from the examiner of the cortical functions may result in problems with identification of important neurological signs appearing during cortical stimulation, and with assessment of the appropriateness of visualization of the examination task by the patient.	Monitoring of the patient face, its mimics, and involuntary movements of the facial muscles at the time of speech arrest during cortical stimulation may be extremely helpful for ruling out both false positive and false negative identification of the speech area and for its precise localization.
Insufficient awakening of the patient from sedation and suboptimal level of his or her conscious may result in poor response to examination tasks and pseudo speech arrest, which may result in false positive identification of the cortical speech area.	Information on the patient sedation level should be integrated with details of his or her response to the examination tasks and those data should be provided both for the surgeon and examiner of the cortical functions.
It may be difficult for the surgeon to assess correctness of the patient response to examination task, since at the same time he or she performs electrical stimulation of the cortex. The examiner of the cortical functions providing the examination tasks for the patient cannot see the nuances of the cortical stimulation performed by the surgeon, which may create problems with precise interpretation of the patient responses.	The information on the cortical stimulation observed by the surgeon through the operating microscope and data on the type of examination task providing for the patient and his or her response should be integrated in real-time. Moreover, this information should be preferably provided not only for the surgeon and examiner of the cortical functions, but for all other members of the surgical team in order to prevent loss of the important information and its correct interpretation.
Even if according to the intraoperative cortical mapping it can be suspected that speech area is localized correctly, it may be difficult for a surgeon to integrate precisely its positioning with the anatomical details of the tumor location.	The information on the electrical cortical stimulation during intraoperative brain mapping should be integrated with the data of intraoperative neuronavigation with three-dimensional visualization of the tumor location.

*According to Yoshimitsu et al.[21] and Sakurai et al.[19]

wireless connections between the image divider and operator monitor to cables was successfully done initially,[21] but simple reduction of the frequency of this transmitter from 2.4 GHz to 1.2 GHz was soon found to be adequate for full resolution of the problem. The wireless modification of IEMAS was used during 34 subsequent awake craniotomies without technical problems during the 12 subsequent months.

Discussion

Precise intraoperative localization of the eloquent cortical areas is of paramount importance during resection of cerebral gliomas. However, the anatomical location has individual variations.[13-15,17,18] Moreover, indolent tumor growth may result in further shift of the functional cortical centers away from the mass. Therefore, intraoperative mapping of cortical and, sometimes, subcortical cerebral structures is essential, which is frequently performed during awake craniotomy with the conscious communicating patient during direct electrical stimulation of the specific brain areas.[1,3,8-10,16,20] Several problems may arise with identification of the cortical speech areas using such technique and require specific solutions (Table 2).[19,21] Particularly, elimination of the anarthria produced by positive motor response of the tongue and face or from the negative motor response of the tongue during cortical stimulation is extremely important for precise evaluation of the language function.[2,10]

Our IEMAS may significantly facilitate cortical brain mapping during awake craniotomy and definitely proved its usefulness.[5,6,11,19] However, sometimes appropriate use suffered from occasional interruption of the connecting cables or detachment. Moreover, the operating surgeon had complained on several occasions of the limited number of intraoperative parameters visualized on the screen of the monitor. While those problems were definitely minor, anxiety and irritation can result for members of the surgical team due to more or less prolonged interruption of the tumor removal. The latter is definitely highly undesirable taking into account the awake condition of the patient.

Modification of the device was directed on installation of the wireless transmitting functions and increase of the number of windows on the operator monitor screen. Some technical problems appearing during initial clinical testing were resolved quickly. Our experience with the modified IEMAS suggests complete elimination of minor problems associated with the previous version. The compact and wireless structure is very convenient to use in the narrow space of the operating room. Further efforts with im-

provement of the IEMAS will include development of a more comfortable user interface and installation of the auto-tracking mechanism in the CCD camera of the patient monitor for automatic correction of its positioning during cortical mapping.

Acknowledgment

These data were presented in part during 32nd Annual International Conference of the IEEE Engineering in Medicine and Biology Society "Merging Medical Humanism and Technology" (August 31–September 4, 2010; Buenos Aires, Argentina).

References

1) Bello L, Galucci M, Fava M, Carrabba G, Giussani C, Acerbi F, Baratta P, Songa V, Conte V, Branca V, Stocchetti N, Papagno C, Gaini SM: Intraoperative subcortical language tract mapping guides surgical removal of gliomas involving speech areas. *Neurosurgery* 60: 67–82, 2007
2) Duffau H: Contribution of cortical and subcortical electrostimulation in brain glioma surgery: methodological and functional considerations. *Neurophysiol Clin* 37: 373–382, 2007
3) Duffau H, Capelle L, Denvil D, Sichez N, Gatignol P, Taillandier L, Lopes M, Mitchell MC, Roche S, Muller JC, Bitar A, Sichez JP, van Effenterre R: Usefulness of intraoperative electrical subcortical mapping during surgery for low-grade gliomas located within eloquent brain regions: functional results in a consecutive series of 103 patients. *J Neurosurg* 98: 764–778, 2003
4) Iseki H, Muragaki Y, Nakamura R, Ozawa N, Taniguchi H, Hori T, Takakura K: Intelligent operating theater using intraoperative open-MRI. *Magn Reson Med Sci* 4: 129–136, 2005
5) Iseki H, Nakamura R, Muragaki Y, Suzuki T, Chernov M, Hori T, Takakura K: Advanced computer-aided intraoperative technologies for information-guided surgical management of gliomas: Tokyo Women's Medical University experience. *Minim Invasive Neurosurg* 51: 285–291, 2008
6) Iseki H, Nambu K: [Intraoperative Examination Monitoring for Awake Surgery (IEMAS)]. *No Shinkei Geka* 33: 1028–1031, 2005 (Japanese)
7) Kayama T, Kumabe T, Tominaga T, Yoshimoto T: Prognostic value of complete response after the initial treatment for malignant astrocytoma. *Neurol Res* 18: 321–324, 1996
8) Kayama T, Sato S: [Definition of individual language related area by awake surgery]. *No To Shinkei* 53: 151–160, 2001 (Japanese)
9) Kim SS, McCutcheon IE, Suki D, Weinberg JS, Sawaya R, Lang FF, Ferson D, Heimberger AB, DeMonte F, Prabhu SS: Awake craniotomy for brain tumors near eloquent cortex: correlation of intraoperative cortical mapping with neurological outcomes in 309 consecutive patients. *Neurosurgery* 64: 836–846, 2009
10) Mikuni N, Miyamoto S: Surgical treatment for glioma: extent of resection applying functional neurosurgery. *Neurol Med Chir (Tokyo)* 50: 720–726, 2010
11) Muragaki Y, Iseki H, Maruyama T, Kawamata T, Yamane F, Nakamura R, Kubo O, Takakura K, Hori T: Usefulness of intraoperative magnetic resonance imaging for glioma surgery. *Acta Neurochir Suppl* 98: 67–75, 2006
12) Muragaki Y, Iseki H, Maruyama T, Tanaka M, Shinohara C, Suzuki T, Yoshimitsu K, Ikuta S, Hayashi M, Chernov M, Hori T, Okada Y, Takakura K: Information-guided surgical management of gliomas using low-field-strength intraoperative MRI. *Acta Neurochir Suppl* 109: 67–72, 2011
13) Ojemann G, Ojemann J, Lettich E, Berger M: Cortical language localization in left, dominant hemisphere. An electrical stimulation mapping investigation in 117 patients. *J Neurosurg* 71: 316–326, 1989
14) Ojemann GA: Neurosurgical management of epilepsy: a personal perspective in 1983. *Appl Neurophysiol* 46: 11–18, 1983
15) Ojemann JG, Miller JW, Silbergeld DL: Preserved function in brain invaded by tumor. *Neurosurgery* 39: 253–259, 1996
16) Otani N, Bjeljac M, Muroi C, Weniger D, Khan N, Wieser HG, Curcic M, Yonekawa T: Awake surgery for glioma resection in eloquent areas: Zurich's experience and review. *Neurol Med Chir (Tokyo)* 45: 501–511, 2005
17) Pouratian N, Cannerstra AF, Bookheimer SY, Martin NA, Toga AW: Variability of intraoperative electrocortical stimulation mapping parameters across and within individuals. *J Neurosurg* 101: 458–466, 2004
18) Quinones-Hinojosa A, Ojemann SG, Sanai N, Dillon WP, Berger MS: Preoperative correlation of intraoperative cortical mapping with magnetic resonance imaging landmarks to predict localization of the Broca area. *J Neurosurg* 99: 311–318, 2003
19) Sakurai Y, Muragaki Y, Okada Y, Nambu K, Iseki H: The development and application of the device for intraoperative examination monitor for awake surgery. *Journal of Tokyo Women's Medical University* 81: 32–40, 2011
20) Sanai N, Mirzadeh Z, Berger MS: Functional outcome after language mapping for glioma resection. *N Engl J Med* 358: 18–27, 2008
21) Yoshimitsu K, Suzuki T, Muragaki Y, Chernov M, Iseki H: Development of modified intraoperative examination monitor for awake surgery (IEMAS) system for awake craniotomy during brain tumor resection. *Conf Proc IEEE Eng Med Biol Soc* 2010: 6050–6053, 2010

Address reprint requests to: Kitaro Yoshimitsu, PhD, Faculty of Advanced Techno-Surgery, Institute of Advanced Biomedical Engineering and Science, Tokyo Women's Medical University, 8-1 Kawada-cho, Shinjuku-ku, Tokyo 162-8666, Japan.
e-mail: kitaro@abmes.twmu.ac.jp

Brain Tumor Pathol (2011) 28:43–51
DOI 10.1007/s10014-010-0002-4

ORIGINAL ARTICLE

Precise comparison of protoporphyrin IX fluorescence spectra with pathological results for brain tumor tissue identification

Takehiro Ando · Etsuko Kobayashi · Hongen Liao · Takashi Maruyama · Yoshihiro Muragaki · Hiroshi Iseki · Osami Kubo · Ichiro Sakuma

Received: 3 March 2010 / Accepted: 13 July 2010 / Published online: 25 December 2010

Abstract Photodynamic diagnosis is used during glioma surgery. Although some studies have shown that the spectrum of fluorescence was efficient for precise tumor diagnosis, previous methods to characterize the spectrum have been problematic, which can lead to misdiagnosis. In this paper, we introduce a comparison technique to characterize spectrum from pathology and results of preliminary measurement using human brain tissues. We developed a spectrum scanning system that enables spectra measurement of raw tissues. Because tissue preparations retain the shape of the device holder, spectra can be compared precisely with pathological examination. As a preliminary analysis, we measured 13 sample tissues from five patients with brain tumors. The technique enabled us to measure spectra and compare them with pathological results. Some tissues exhibited a good relationship between spectra and pathological results. Although there were some false positive and false negative cases, false positive tissue had different spectra in which intensity of short-wavelength side was also high. The proposed technique provides an accurate comparison of quantitative fluorescence spectra with pathological results. We found that spectrum analysis may reduce false positive errors. These results will increase the accuracy of tumor tissue identification.

Keywords 5-Aminolevulinic acid · Protoporphyrin IX · Fluorescence spectra · Photodynamic diagnosis

T. Ando (✉) · E. Kobayashi · H. Liao · I. Sakuma
Department of Bioengineering, Graduate School of Engineering, The University of Tokyo, Engineering building No.14, Room 722, Hongo 7-3-1, Bunkyo, Tokyo 113-8656, Japan
e-mail: take_and_o@bmpe.t.u-tokyo.ac.jp

T. Maruyama · H. Iseki · O. Kubo
Department of Neurosurgery, Neurological Institute, Tokyo Women's Medical University, Shinjuku, Tokyo 162-8666, Japan

Y. Muragaki · H. Iseki
Institute of Advanced Biomedical Engineering and Science, Tokyo Women's Medical University, Shinjuku, Tokyo 162-8666, Japan

Introduction

Over recent decades, photodynamic diagnosis (PDD) has been studied for intraoperative tumor diagnosis, especially glioma. PDD uses autofluorescence or endogenous fluorescence materials [1–4], and the technique can be easily applied for clinical practice because the system is simple. In a number of clinical studies, 5-aminolevulinic acid (5-ALA)-induced protoporphyrin IX (PpIX) fluorescence has been used for intraoperative tumor diagnosis. Although 5-ALA and PpIX are natural substances produced by the human body, orally administrated 5-ALA accumulates in tumor cells and is converted to PpIX by heme biosynthesis. Accumulation of 5-ALA in a tumor cell may be caused by a damaged blood brain barrier (BBB) or iron (Fe)-metabolic enzyme defect, such as ferrochelatase [5]. However, the exact mechanism is still unknown.

Stummer et al. [1–3] introduced the use of the fluorescence surgical microscope to examine PpIX fluorescence for intraoperative tumor detection. They reported that some regions of brain and tumor tissue have different fluorescence characteristics (intensity and color) and assessed these tissues pathologically. Although this approach was appropriate for fluorescence-guided surgery, fluorescence measurement was not quantitative. A recent study of quantitative fluorescence measurement showed that PpIX spectrum shape is important to precisely detect tumor and

diagnose malignancy [6]. Another group reported that ultraviolet (UV) laser and white light reveal differences in the autofluorescence spectra between tumor and normal brain tissue [7, 8]. Although these quantitative studies found characteristic tumor tissue spectra when comparing them with pathological results, the comparison methods used have the following limitations. First, there is a possibility that a spectrum measurement point is different from a pathology examination point. This means that a spectrum characterization may not be correct. Second, because the spectrum measurement was performed after staining or fixation with formalin, the measured spectrum may be different from that of the raw tissue. To use the result in situ, raw tissue spectrum measurement is necessary. Finally, although tumor margin characterization is necessary for precise resection, these methods cannot determine spatial changes in spectra.

To solve these problems, we developed a spectrum scanning system that enables acquisition of raw tissue spectra distribution. Furthermore, our novel protocol makes it possible to precisely compare spectra with pathological results. In this paper, we introduce the technique we devised and present results of preliminary measurements.

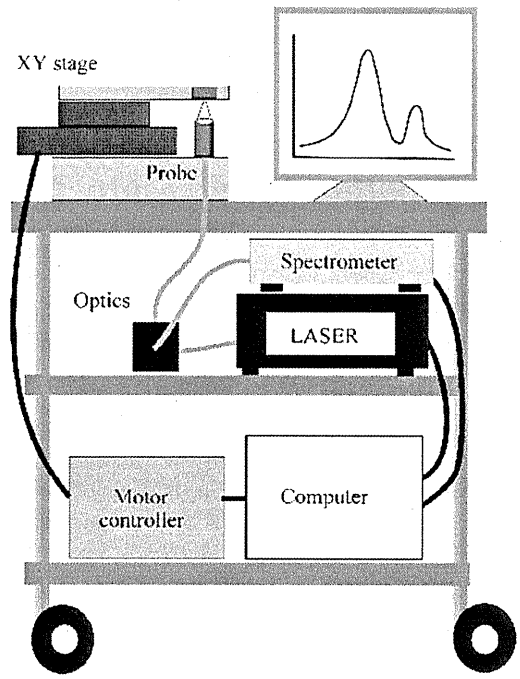

Fig. 1 Overall view of the measurement system

Materials and methods

Measurement system

A spectrum-scanning system for 5-ALA-induced PpIX fluorescence was especially designed for both fluorescence measurement and fluorescence spectra comparison with pathological results. The system consists of an excitation laser (VLS405-SA3, Digital Stream), a spectrometer (WTC-111E B&W, TEK Inc.), optics, and a computer (Fig. 1). The excitation laser emits 405 nm of UV light, and the maximal output power is 15 mW. The spectrometer wavelength range is 300–850 nm. The measurement probe uses a coaxial optical system. All light paths are connected with optical fibers (core diameter 365 μm, multimode), and a dichroic mirror is used to separate excitation light and fluorescence. To insert a dichroic mirror in the light path, three collimator lenses are mounted to a cubic box. Angles and positions of all collimator lenses and the dichroic mirror angle can be adjusted to improve the coupling efficiency of the light. It is also equipped with a long-pass filter to separate strong reflected excitation light from the fluorescence signal. There are two achromatic lenses at the tip of the probe. The focal length of the fiber side lens is 19 mm, the object side is 30 mm, the working distance is 21.7 mm, and the lens diameter is 12.5 mm. The measurement spot diameter is evaluated using a phantom, the optical character of which is designed to match that of brain tissue. As a result, the system's measuring diameter is estimated as 0.8 mm.

To measure fluorescence spectra spatial changes, the measurement probe is fixed under an *XY* stage (SGSP20-35XY, Sigma Koki), and the sample tissues are then moved. A removable tissue holder that has a square 5-mm hole is set on the stage. One corner of the holder hole is cut down to make a shape mark. Because the holder location is registered to the *XY* stage coordinates, it is possible to follow the measuring position. In this study, spectra of 58 points were acquired from each sample tissue.

Measurement protocol

To accurately compare spectra with pathological results, we devised the following measurement protocol:

1. Resected tissue was gently put in the measurement system tissue holder.
2. The spectrum of each point was measured by the system, and data were processed automatically.
3. After measurement, the tissue and the holder were put in liquid nitrogen to freeze the tissue.
4. The frozen tissue was taken out of the holder and sectioned using conventional methods.
5. The sectioned tissue was stained with hematoxylin–eosin (H&E).

Sectioning and staining were performed by a pathologist. Spectrometer exposure time and the laser power were